A model and sounding rocket simulation tool with *Mathematica*®

Tiago Miguel Oliveira Pinto
tiagomopinto@tecnico.ulisboa.pt

Instituto Superior Técnico, Lisboa, Portugal

November 2015

Abstract

This work aims to simulate trajectories from model to sounding rockets taking into account the wind and the atmospheric boundary layer. The developed tool is also capable to forecast the most probable landing region and perform rocket design optimization using Monte Carlo methods. A study of the atmospheric boundary layer is carried out and are considered three wind profiles that take into account the atmospheric conditions and the terrain type in the launch site. Presenting the developed tool's flexibility, a Monte Carlo simulation is performed in order to deduce the dispersion of the landing sites due to the wind parameters' uncertainties. Owing to the *Mathematica*®'s potentialities, the developed tool allows to define any number of stages, with external or internal boosters in the first stage, and to easily modify the required models to compute the trajectory or to implement new ones in the database.

A test simulation using a two-stage model rocket was performed and the results showed a large dependence of the trajectory on the wind profile. Considering the defined uncertainties from the wind speed and direction, as well from the surface type, they presented a strong influence on the dispersion of the landing sites.

Keywords: Trajectory Simulation, Model Rocketry, Atmospheric Boundary Layer, Monte Carlo.

1. Introduction

This paper focuses on passively controlled rockets, whose trajectories are influenced by the wind that changes according the land surface [1] and time of the day [2]. Thus, if the wind profile is foreseen under given conditions, the simulations' errors can be minimized and simulations in different conditions can provide to users important information to help selecting the site and day of the launch to achieve successful flights. Sounding rockets consist of one or more stages (propelled by solid or liquid fuel) carrying a scientific payload in order to study the atmosphere and carry out microgravity research between 40 km to 2000 km height [3]. From 40 km to 200 km, these rockets are specially interesting because neither balloons nor low-earth satellites can reach these altitudes. Hence, allowing the developed tool to simulate trajectories of fin-stabilized sounding rockets up to these heights, brings additional useful applications to our project.

Although the simulations from the developed tool may cost a larger processing time due to the interpreted language of *Mathematica*® [4], it presents valuable features as: simulation of trajectories from micro to sounding rockets (and even any type of missiles); flexibility to change easily a certain input in a given model and figure out its influence in the trajectory; freedom to edit or implement new functions and values into the simulator's database; and process the resulting data in order to obtain further conclusions. Besides these, are also embedded other basic features such as multi-staging, boosters, launch direction and atmospheric, wind and drag coefficient models. The simulator does not include a modeling interface, however, it allows to define a versatile rocket model that is functional to every type of rockets. This is accomplished by using a default scheme of lists structured according the number of stages and boosters. Therefore, this structure of lists, allied to the simulator code, allows the rocket model to have any number of stages, although this scheme of lists must always be respected so that the program runs properly. As this tool is developed under a modular programming philosophy, the necessary inputs to the trajectory function are independent from each other. Hence, all of them can be easily modified without worrying about the other models. This allows to run several simulations under very different conditions and compare their impact in the trajectory. Two databases are already

implemented as default, one for the rocket's motors and another for the atmospheric models. The databases are defined in a way that simplifies the access to the data and their properties. Besides, another models can be joined in the databases to expand the options to use during the simulations. The developed simulator also allows the user to compute trajectories in loop, changing a determined group of parameters. This procedure employs the Monte Carlo methods enabling the formulation of further studies. These analysis may consist of calculations to determine a probable landing region giving certain parameters' uncertainties or a rocket design optimization evaluating the combination of possible values for the components that achieve the desired goal in the trajectory.

2. Theoretical background

A rocket is stable if its Center of Pressure (CP) is behind the Center of Mass (CM) (seeing from the nose to the tail of the rocket) [5]. The CP is the point where acts the resultant aerodynamic force produced by the air pressure and moves toward the nose with increasing angle of attack (α). This force, when there is an angle of attack, may be decomposed as an axial and normal force where the latter creates a moment about the CM of the rocket. In stable conditions, this moment produces a damped oscillating movement between the air flow direction until the rocket flies without angle of attack and the normal force vanishes [5]. The arm of the moment is the length between the CM and the CP, called *static margin*. Decreasing the static margin until the CP overtakes the CM, makes the rocket unstable because the resulting moment reverses its direction. In this situation, if a perturbation deviates the rocket from the air flow direction, the aerodynamic moment will amplify the disturbance causing the rocket to spin and crash. With a larger static margin, however, the rocket may become *overstable* and reaches a lower apogee because it turns sooner to the wind [5]. This effect, called *weathercocking*, is due to the contributions of the rocket and wind's velocities ($\mathbf{v}$ and $\mathbf{w}$, respectively) that define the direction and intensity of the true air speed as

$$\mathbf{v_t} = \mathbf{v} - \mathbf{w}\,. \tag{1}$$

The angle of attack is maximum when the rocket leaves the guiding rods and is found by (see Fig.(1))

$$\alpha = \arccos \frac{\mathbf{v}\cdot\mathbf{v_t}}{\|\mathbf{v}\|\|\mathbf{v_t}\|}\,. \tag{2}$$

Note that $\mathbf{v}$ may describe other angles in respect to the ground, so that Figure 1 no longer depicts a right triangle.

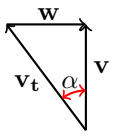

Figure 1: Air speed components.

2.1. Wind

The lowest layer of the troposphere is directly influenced by the ground surface characteristics. Therefore, a wind speed profile is worth to be implemented since its effect will be noticed, mainly, in the trajectory of small and medium model rockets. This layer is known as the Atmospheric Boundary Layer (ABL) and its thickness may change from about a hundred meters to a few kilometers varying in time and with geographic region [6]. The bottom 10% of the ABL is named the Surface Layer (SL) with, in average, 100 m height [7] which makes the ABL about 1 km thick.

Above the ABL stays the *free atmosphere*, a more stable region where the frictional influences of the surface can be ignored and the wind is nearly geostrophic [6]. This wind, moving parallel to the isobars, results from the balance between the Coriolis and the pressure gradient forces [8]. Considering only geostrophic balance, which is the case of a *barotropic* atmosphere, the wind is constant with height and its intensity can be assumed as equal to the one at the top of the ABL.

Regarding atmospheric stability, the ABL is classified in three different classes: neutral, stable and unstable. A neutral atmosphere implies an adiabatic lapse rate and no convection which is the case of a partially or highly cloudy atmosphere that may reduce the insolation at the surface [6]. Stable conditions occur mostly at night but can also appear when the ground surface is colder than the surrounding air. An unstable atmosphere is formed in clear weather during the day when there is high radiation from the sun causing ascending heat transfer. These conditions influence the wind profile and must be taken into account due to convective effects.

From measurements of the wind speed, the literature [9] presents the following wind profiles modeled considering the entire ABL and its stability:

$$u(z) = \frac{u_0^*}{\kappa}\left[\ln\left(\frac{z}{z_0}\right) + \frac{4.7z}{L}\left(1-\frac{z}{2h}\right) + \right.$$
$$\left. + \frac{z}{L_{MBL}} - \frac{z}{h}\left(\frac{z}{2L_{MBL}}\right)\right]\,, \tag{3}$$

for stable conditions,

$$u(z) = \frac{u_0^*}{\kappa}\left[\ln\left(\frac{z}{z_0}\right) + \frac{z}{L_{MBL}} - \frac{z}{h}\left(\frac{z}{2L_{MBL}}\right)\right]\,, \tag{4}$$

for neutral conditions, and

$$u(z) = \frac{u_0^*}{\kappa}\left[\ln\left(\frac{z}{z_0}\right) - \psi\left(\frac{z}{L}\right) + \frac{z}{L_{MBL}} - \right.$$
$$\left. - \frac{z}{h}\left(\frac{z}{2L_{MBL}}\right)\right], \quad (5)$$

for unstable conditions, where h is the ABL depth, z_0 is the surface roughness length, κ is the von Kármán constant, L_{MBL} is the length scale in the middle of the ABL for its respective conditions, u_0^* is the local surface friction velocity near the ground, L is the Obukhov length and ψ is a stability correction for the SL.

The surface type influences z_0 which is quantified and can be obtained from Table 1.

Surface type	z_0 (cm)
Sand	0.01...0.1
Cut grass (~ 0.01 m)	0.1...1
Small grass, steppe	1...4
Uncultivated land	2...3
High grass	4...10
Coniferous forest	90...100
Uptown, suburbs	20...40
Downtown	35...45
Big towns	60...80

Table 1: Surface roughness values for different land surfaces [1].

The Obukhov length (L) represents the thickness near the surface in which the shear stress dominates over the buoyancy effects in generating turbulence. This parameter is hard to estimate since we get considerable errors even for measurements taken hundreds of meter above the surface. Nevertheless, if the atmospheric stability is deduced qualitatively from the weather conditions and time of day (as described before in the section), we get to know which wind profile to use and a value for L can be estimated from Table 2.

2.2. Trajectory

The launch site is a non-inertial topocentric-horizon coordinate frame with the x axis pointing southward and the y eastward. Thus, as this is a right-handed coordinate frame, the z axis points upward collinear with the Earth's radius direction (or zenith). The total acceleration, in the Earth-centered inertial coordinate frame, is given by [10]

$$\mathbf{a} = \mathbf{a_o} + \tfrac{\partial^2 \mathbf{r}}{\partial t^2} + \tfrac{\mathrm{d}\boldsymbol{\Omega}}{\mathrm{d}t} \times \mathbf{r} + 2\boldsymbol{\Omega} \times \tfrac{\partial \mathbf{r}}{\partial t} + \boldsymbol{\Omega} \times (\boldsymbol{\Omega} \times \mathbf{r}), \quad (6)$$

where $\boldsymbol{\Omega}$ is the Earth's angular velocity, $\mathbf{r}$ is the position of the rocket relative to the local frame and

Obukhov length interval (m)	Stability class
$10 \leq L \leq 50$	Very stable
$50 \leq L \leq 200$	Stable
$200 \leq L \leq 500$	Near stable
$\lvert L\rvert \geq 500$	Neutral
$-500 \leq L \leq -200$	Near unstable
$-200 \leq L \leq -100$	Unstable
$-100 \leq L \leq -50$	Very unstable

Table 2: Atmospheric stability classes according to intervals of Obukhov length, L [9].

$\mathbf{a_o}$ is the linear acceleration of this frame given as $\boldsymbol{\Omega} \times (\boldsymbol{\Omega} \times \mathbf{R_o})$, where $\mathbf{R_o}$ is the position of the local frame's origin relative to the Earth's center. The rocket's velocity seen from an observer at the launch site is $\mathbf{v} = \frac{\partial^2 \mathbf{r}}{\partial t}$, where the partial derivative stands for the time derivative of $\mathbf{r}$ with reference to the local frame. The term $\frac{\mathrm{d}\boldsymbol{\Omega}}{\mathrm{d}t} \times \mathbf{r}$ is the angular acceleration of the moving frame, $2\boldsymbol{\Omega} \times \frac{\partial \mathbf{r}}{\partial t}$ is the Coriolis acceleration and $\boldsymbol{\Omega} \times (\boldsymbol{\Omega} \times \mathbf{r})$ is the centripetal acceleration. In order to get the trajectory seen by an observer at the launch site, we must write these vectors in the local frame coordinates.

After using the momentum conservation (taking into account the loss of mass and the external forces) and applying (6), the trajectory equation results in

$$m\frac{\partial^2 \mathbf{r}}{\partial t^2} = -m\mathbf{a_o} - m\frac{\mathrm{d}\boldsymbol{\Omega}}{\mathrm{d}t} \times \mathbf{r} - 2m\boldsymbol{\Omega} \times \frac{\partial \mathbf{r}}{\partial t} -$$
$$-m\boldsymbol{\Omega} \times (\boldsymbol{\Omega} \times \mathbf{r}) + \mathbf{T} + \mathbf{D} + \mathbf{W}, \quad (7)$$

where m is the rocket's mass, $\mathbf{T}$ is the thrust, $\mathbf{D}$ is the drag and $\mathbf{W}$ is the weight. Solving (7), the position of the rocket seen from the launch site can be obtained.

The thrust is always aligned with the rocket's longitudinal axis as the rocket is not steerable. Since the rocket may fly with angle of attack until it stabilizes and the thrust becomes collinear with the true speed vector, the effective propulsive force may be lower in this direction. Therefore, the adopted model to the thrust force is

$$\mathbf{T} = \mathrm{T}_p \cos\alpha \, \frac{\mathbf{v_t}}{\|\mathbf{v_t}\|} \quad (8)$$

where T_p is the propulsion from the motors' thrust profile. The aerodynamic force is assumed to be merely the drag since the rocket only flies with angle of attack during a short interval of time after the launch (or after any perturbation) and it describes a low amplitude oscillation. The lift that is produced during these moments contributes essentially to stabilize the rocket, its average is considered to

be zero, and its effect can be implemented as described in Section 2.3. Thus, the aerodynamic force comes

$$\mathbf{D} = \frac{1}{2}\rho\|\mathbf{v_t}\|\, SC_D\mathbf{v_t}\,, \tag{9}$$

where ρ is the air density, S is the reference area (usually chosen as the maximum sectional area of the rocket or, after the apogee, the reference area of the recovery device) and C_D is the drag coefficient. The weight points to the Earth's center and is found by

$$\mathbf{W} = -\frac{\mu_\oplus m}{(R_0+z)^2}\,\mathbf{z}\,, \tag{10}$$

where $\mu_\oplus = 3.986\times10^5\,\mathrm{km^3\,s^{-2}}$ is the Earth's gravitational parameter and $\mathbf{z}$ is the unit vector of the vertical coordinate.

During the launch, when the rocket is constrained by the guiding rods, the drag and weight normal to the launch direction are counterbalanced by the rod's reaction and only the tangential forces to the rods contribute to the launch. Thus, the last three terms in (7) become

$$\mathbf{T}+\mathbf{D}+\mathbf{W} = -\tfrac{1}{2}\rho\|\mathbf{v}\|\, SC_D\mathbf{v} + (\mathrm{T}_p + \mathrm{W}\sin El)\mathbf{e_l}\,, \tag{11}$$

where $\mathbf{e_l}$ is the unit vector of the rods' direction determined by the launch elevation (El) and azimuth (Az) as

$$\mathbf{e_l} = (\cos El\cos Az, \cos El\sin Az, \sin El)\,. \tag{12}$$

2.3. Dynamic stability

After leaving the platform, and when a disturbance occurs, the rocket acquires an angle of attack that will gradually decrease and force it to oscillate about the true air speed direction. To generate this damped oscillating movement, we conclude the rocket is subjected to two moments [11]: a stabilizing (or restoring) moment and a damping moment.

The stabilizing moment comes from the normal aerodynamic force acting on the CP which causes the rocket to rotate about the CM since these points must distance from each other by the static margin. Therefore, assuming small angles of attack, the stabilizing moment is found by

$$M_s = \frac{1}{2}\rho V^2 SC_{N_\alpha}\alpha(\mathrm{x}_{cp}-\mathrm{x}_{cm})\,, \tag{13}$$

where x_{cm} and x_{cp} are, respectively, the rocket's CM and CP distances from the reference point (often considered as the nose tip, which we also consider throughout this work), V is the flow velocity and C_{N_α} is the rocket's normal force coefficient derivative .

One source of the damping moment results from the aerodynamic resistance of the air while the rocket is rotating [11]. During the rotation, the angle of attack of each part of the rocket changes due to the tangential velocity of this motion. Like the stabilizing moment, only the normal force of this additional resistance contributes to dampen the rotation. Thus, since the aerodynamic damping moment (M_{d_a}) is determined by summing all the elemental moments along the rocket [11], we get [12]

$$M_{d_a} = \frac{1}{2}\rho VS\dot\alpha\sum_{i=1}^{n} C_{N_{\alpha_i}}(\mathrm{x}_{cp_i}-\mathrm{x}_{cm})^2\,, \tag{14}$$

where n is the total number of components of the rocket that contribute to this moment.

The other contribution to the damping moment comes from the Coriolis acceleration due to the change of the gas flow through the nozzle, also called *jet damping*, given by [11]

$$M_{d_j} = \dot\alpha\dot m(\mathrm{x}_{nozzle}-\mathrm{x}_{cm})^2\,, \tag{15}$$

where x_{nozzle} is the nozzle distance from the reference point and $\dot m$ is the rocket's burning rate.

The governing equation for the motion of the angle of attack, assuming the rotation is two dimensional (in the plane formed by the rocket's velocity and wind vectors), is found by the angular momentum knowing that the stabilizing and damping moments counteract the rotation. Thus, we get

$$-M_s - M_{d_a} - M_{d_j} = \dot I\dot\alpha + I\ddot\alpha\,, \tag{16}$$

where I is the transversal moment of inertia relative to the CM. Applying (13), (14) and (15) in (16), we get a second-order differential equation that represents a damped harmonic oscillator (considering the rocket is stable) giving the angle of attack.

3. Rocket trajectory simulator

The simulator's main function, which integrates the trajectory equations, receives all the required inputs and calls the function that computes every parameter of the rocket over time. These properties are determined by combining the data of the several stages regarding the developed structure that gathers the data of the rocket and considering the instants of the ignitions and ejections. The most relevant inputs are the rocket, density, wind and C_D models that, since they are external parameters, the user is allowed to define or change them according to his needs. The outputs from the simulation are three functions giving the position (one for each cartesian coordinate) plus a function giving the angle of attack. These are computed in three steps: one for the constrained trajectory due to the guiding rod, another for the climbing phase and the last one for the recovery trajectory. The angle of attack starts to be computed only in the second phase, since it is when the rocket suffers the first

perturbation from the wind. After this process, the three parts of the trajectory are merged together and, having these time dependent functions, it is possible to determine its derivatives and get other flight data such as total velocity, total acceleration, Mach and flight path angle.

3.1. Rocket assembly

The proposed structure for a general multi-stage rocket developed in the present thesis is shown in Figure 2. Although the figure represents a three-

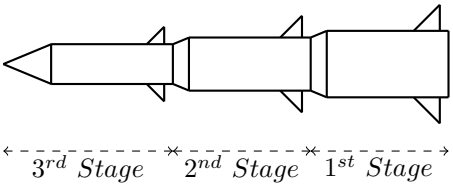

Figure 2: Multi-stage rocket design.

stage rocket, this structure can be extended to any number of stages and was developed with the goal of modeling several types of rockets, specially the most common. For each stage the fundamental components are: a connector (or nose, in the case of the last stage), a body tube and fins. Internally, it is only considered the motors since data from additional components can be joined with the body tube properties. In the first stage the rocket can also be supplied with external boosters in order to achieve parallel staging.

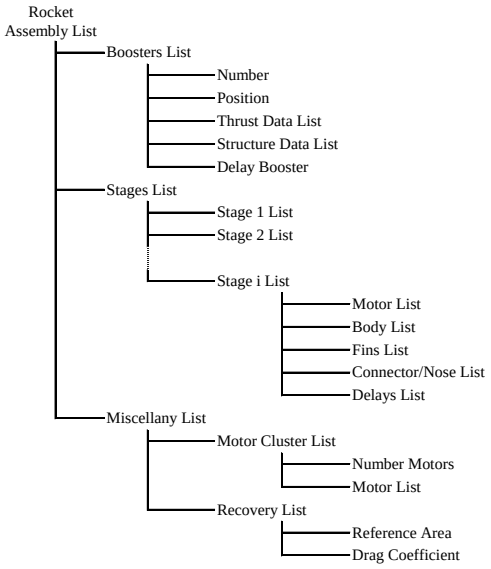

Figure 3: Rocket assembly list structure.

The defined structure of lists enables to access easily the rocket's data and to be quickly processed by the simulator. This structure has three major lists concerning, respectively, the external boosters, the stages and the recovery system plus the motor cluster in the first stage (see Figure 3). The stages list contains as many lists as the number of stages. Each one of these lists holds other lists respecting the stages components plus a list to indicate the time intervals between the discharges. All of this data (dimensions, mass, CM, inertia, CP and C_{N_α}) can be defined manually by the user or, in some cases, estimated by default functions implemented in the simulator.

3.2. Developed models

The atmospheric model stored in the database is the CIRA-86 which gives pressure and temperature data up to 120 km (the latter is also dependent on the latitude and the month of the year). This or other atmospheric models can take into account the conditions at the launch site using developed functions that match the measured pressure and temperature at the corresponding altitude with the values from the model at higher altitudes (see Figure 4a). One of this functions also determines the density from the equation of state.

The developed wind model uses the ABL profiles (taking into account the atmospheric stability) that approximate the wind data also provided in the CIRA-86 model at higher altitudes. If desired, the wind may be constant above the ABL. This model requires local wind speed, its respective measurement altitude, the terrain's specification and the downwind direction. Wind gusts can also be implemented providing their intensity and the instants of the respective perturbations as another input of the trajectory function. These disturbances are simulated considering they change instantly the angle of attack to another value determined by the rocket and wind gust's velocities at the perturbation's instant. After that moment, the simulator computes new oscillations for the angle of attack (see example in Figure 4b).

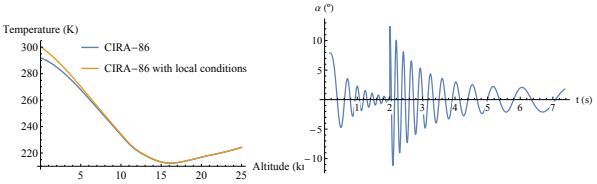

(a) Temperature profiles for the CIRA-86 model.

(b) Angle of attack until the apogee with a wind gust perturbation.

Figure 4: Temperature and angle of attack models.

The simulator also provides a drag coefficient model that takes the structure of lists respecting the rocket's data and determines the drag coefficients for each one of the external components depending on Mach and Re_x. Then it gathers all the

coefficients to compute the rocket's C_D in respect to its reference area. Using this drag coefficient model, we are considering that all the components contribute to the skin friction drag but the pressure drag comes only from the nose, connectors and fins (due to the normal surface facing the flow). In this model the rocket's nose is the only wave drag source whose effect is implemented by a fitted function in the transonic regime under M = 1 and by an empirical function above this Mach. The final drag coefficient function for the conical nose, including the wave drag, is represented in Fig.(5).

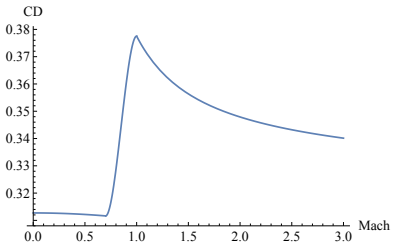

Figure 5: Conical nose drag coefficient with Mach.

3.3. Validation of the tool

The developed tool requires validation in order to assure the simulator meets the specifications and correctly computes the expected output. This may be performed by comparing our results with a known analytic solution from a specific launch.

One of developed tests consists in determine the error presented between the altitude from a vertical sounding rocket launch and the tool's output under the same conditions. The analytical solution requires that these conditions correspond to a case without atmosphere and the effects of the Earth's rotation, constant thrust and constant acceleration of gravity. The obtained relative error over time (until the burnout) is represented in Fig.(6). It can

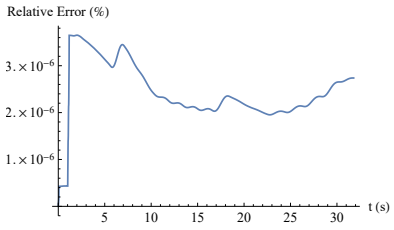

Figure 6: Altitude's relative error between analytical and numerical solution until the burnout.

be observed that the error presents values in the order of magnitude of 10^{-6}%. Although this error gives reasonable results under the mentioned conditions, more tests should be performed in order to increase the confidence in the solutions from the developed simulator.

To check the drag effect, we can make a terminal velocity test for a given rocket in free fall after the apogee. From an equilibrium between the gravitational force and the drag force, we can find the terminal velocity and conclude that if the rocket loses mass, it must reach a slower velocity. In Fig.(7) it is represented this quasi-static process computed by the simulator. As we can see, the rocket tends asymptotically to a new terminal velocity, as expected.

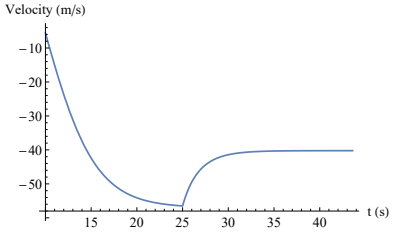

Figure 7: Descent velocity from a vertical launch in which the rocket loses mass at 25 s.

4. Test results

In Fig.(8) are presented the results from the assembling of a two-stage model rocket. Since model rockets reach lower velocities and apogees, they are

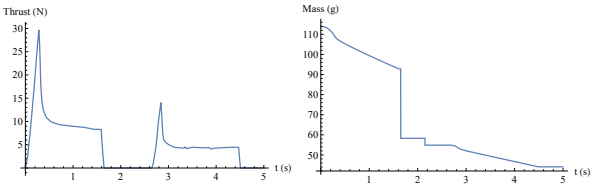

(a) Thrust.

(b) Mass.

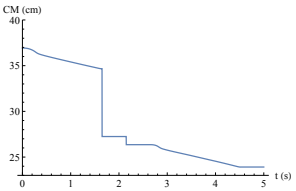

(c) CM relative to the nose tip.

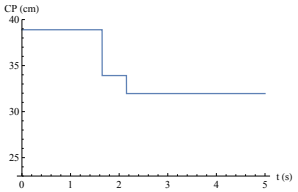

(d) CP relative to the nose tip.

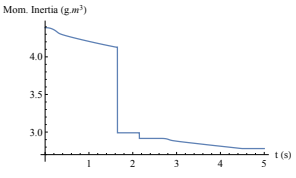

(e) Transversal moment of inertia relative to the CM.

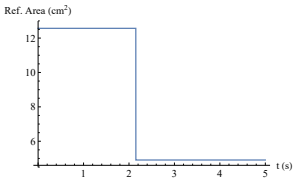

(f) Reference area.

Figure 8: Model rocket properties' functions.

suitable to observe the effects of the wind and the

ABL on the trajectory simulation. Due to the first discontinuity shown in Fig.(8b), Fig.(8b), Fig.(8c), Fig.(8d) and Fig.(8e), we can see that the first stage's structure (not considering the connector) is discarded at the first burnout. Also in these figures, during the coasting phase (lasting 1 s), we see the connector's discharge represented by the second discontinuity. Except from these sharp changes, the rocket maintains its properties during coasting, leading the mentioned figures to match with Figure 8a when there is no thrust between the burnings. The reference area is defined as the largest cross section of the rocket (without considering boosters, for other cases) at each instant. This definition agrees with Figure 8f, where it shows the rocket's reference area changing nearly 2 s after the launch, which is the instant when the connector is discarded and the rocket loses its largest sectional area. Comparing Figures 8c and 8d, we conclude this rocket is always stable since the CM, instead of the CP, is closer to the nose all the time. Hence, the rocket is well assembled and able to be used in a trajectory simulation.

4.1. Trajectory simulation

From the previous rocket, we get the trajectory depicted in Fig.(9). This rocket is launched vertically (in order to be easily observed the deviation from the launch direction) under a neutral atmosphere with a constant wind speed above the ABL, blowing northeastward in a high grass terrain.

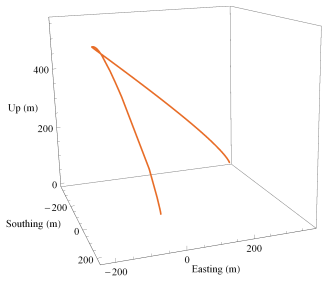

(a) 3D trajectory.

(b) Trajectory profile.

Figure 9: Model rocket trajectory with a vertical launch and a neutral ABL; Parachute ejection at the apogee.

In this trajectory the weathercock effect is observable. Since the wind blows northeastward, the rocket climbs in the opposite direction (southwestward) to follow the true air speed. Although this effect increases smoothly with altitude due to the ABL, we can see a slightly discontinuity in the upward flight path around 200 m of altitude. This happens because the weathercock is enhanced during the coasting time, between the first burnout and the second ignition, as the rocket decreases its velocity. During the recovery phase, the rocket slowly descends toward the downwind direction. Hence, it surpasses the launch site and lands 380 m north and 382 m east away from that place (coordinates taken from the simulator). The influence of the ABL is also observable during the recovery phase in which the trajectory describes a smooth curvature since the wind speed is decreasing as the rocket falls. If the wind was constant with altitude, the recovery trajectory would describe a linear path.

In Fig.(10) the flight data from this launch is represented. From Fig.(10a) we deduce that the rocket reaches the apogee at about 560 m of altitude and lands 120 s after the lift off. Observing when the vertical velocity turns negative, in Fig.(10b), we conclude that the apogee is reached at 9.5 s, approximately. As already mentioned, we also see that the rocket decreases velocity due to the coasting between stages. This is also observable from the Mach number, in Fig.(10d), which remains subsonic

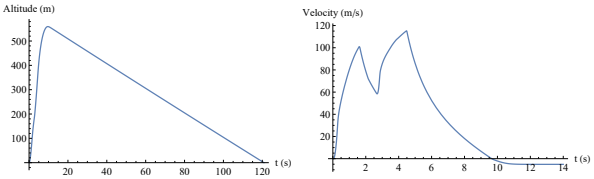

(a) Profile of altitude vs time.

(b) Profile of vertical velocity vs time.

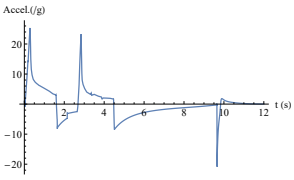

(c) Longitudinal acceleration vs time.

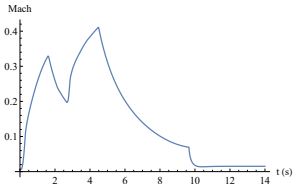

(d) Mach vs time.

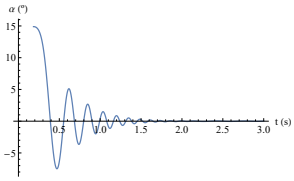

(e) Angle of attack vs time.

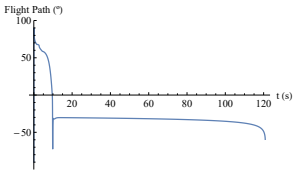

(f) Flight path angle vs time until the landing.

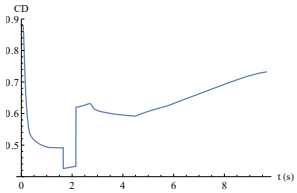

(g) Drag coefficient vs time until the apogee.

Figure 10: Vertical model rocket launch flight data.

throughout the entire flight.

During the burnings, in Fig.(10c), the acceleration describes a profile similar to the thrust (see Fig.(8a)). However, it is decreasing over time as the rocket gains velocity, which increases the drag opposing the thrust force. In contrast, when the rocket is not burning, the acceleration is negative and increases over time (decreases in absolute value) because the velocity is decreasing. The peak acceleration at 9.5 s results from the parachute ejection.

The angle of attack, in Fig.(10e), shows the rocket rapidly damps its oscillations and follows the true air speed during the majority of the ascending flight. During the first instants the angle of attack is not computed because its model receives the impulse to start the oscillations only when the rocket leaves the guiding rod.

From Fig.(10f), we can see the flight path angle as 90° at the ignition since the launch is vertical. This angle decreases until the apogee due to the weathercock effect that causes a curvature in the trajectory. Reaching the apogee, the flight path angle becomes negative because the rocket starts to descend. There is a peak value of about −90° since the rocket reverses its direction and stabilizes in a 30° slope, approximately, toward the ground due to the drag force on the parachute. As the rocket descends, the flight path decreases, which means the velocity is becoming steeper. This fact agrees with the curvature described by the trajectory due to the ABL, observed in Fig.(9).

The drag coefficient, in Fig.(10g), is dependent on the Reynolds and the Mach numbers. Therefore, when the velocity is increasing, the drag coefficient decreases its value due to the skin friction drag. Inversely, as the velocity decreases, the drag coefficient starts to increase. When the first stage is discarded, the C_D decreases instantaneously because the rocket loses a great source of drag. On the other hand, when the connector is discarded, although it is lost another source of drag, the C_D increases significantly. This happens because this is the instant when the reference area becomes smaller and the C_D has to change in order to be given in respect to another section.

5. Stochastic methods

Many of the parameters required to determine the trajectory cannot be known (or well defined, at least) and the measured data may vary randomly, presenting some uncertainties. Therefore, in order to analyze the outcome of several uncertain scenarios, it lead us to perform simulations that rely on repeated random sampling and statistical analysis to compute the results, known as Monte Carlo simulations [14]. To get the outcome due to the uncertainties, we must identify a suitable probability distribution for each input parameter from which a set of data is randomly generated. Then, all the possible combinations between the created data correspond to the inputs given in each trajectory simulation, which highly increases the number of simulations if we are studying many parameters with a large sample. Therefore, since we do not own such great computational resources to minimize the simulation time, a better approach to perform *what if* simulations in which it is analyzed the outcome from the uncertainties of only two or three parameters with smaller samples.

In the following simulations we use a single-stage high power rocket in order to present results from a more powerful rocket.

5.1. Landing site uncertainties

After studying the uncertainties presented in the landing site due to the parameters required to determine the atmospheric and C_D models, we concluded that only the wind speed and direction measured at the launch site and the surface roughness length (terrain type) presented a large uncertainty in the results under the defined conditions. Therefore, these are the three parameters to taking into account in the Monte Carlo simulation. The wind speed and direction data are randomly generated from a normal distribution, creating a sample of two hundred points for each parameter. On the other hand, only the worst case scenarios for the roughness length are considered (for a high grass terrain). Also, in order to reduce the simulation time, and since it is not expected to impact the results much, a mean C_D is determined from a single simulation under the same conditions. The resulting landing sites dispersion is represented in Fig.(11). Since

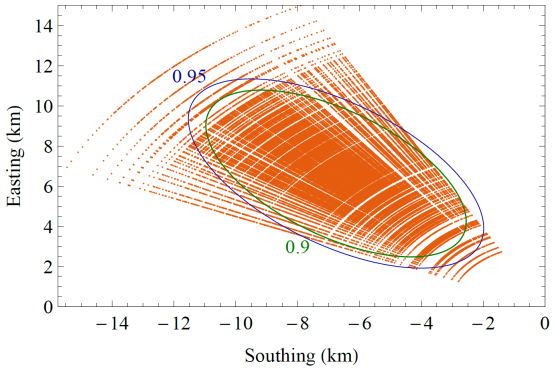

Figure 11: Landing positions and respective confidence ellipses from the Monte Carlo simulation.

the rocket follows the wind speed direction, it is expected the uncertainties from the local wind velocity and the surface roughness length (both only influencing the wind intensity) change the landing site along this direction, describing a straight line.

Analogously, the changes in the wind direction, due to its uncertainties, make the landing points to describe an arc of a circumference that gets larger as the distance to the launch site increases.

The dispersion of the landing points, in Fig.(11), clearly shows the influence of the normal distributions used to generate the local wind direction and speed applied in each iteration. Since a mean of 45° was defined for the wind direction's normal distribution, the orange dots are heavily concentrated along the northeast direction. In the same way, the rocket lands less often apart from the northeast direction as there are fewer inputs that deviate more from the mean. Also due to this principle, the wind speed uncertainties contribute to the lower density of points near the closest and furthest distances from the launch site. This pattern can also be seen in Fig.(12) where the probability density function

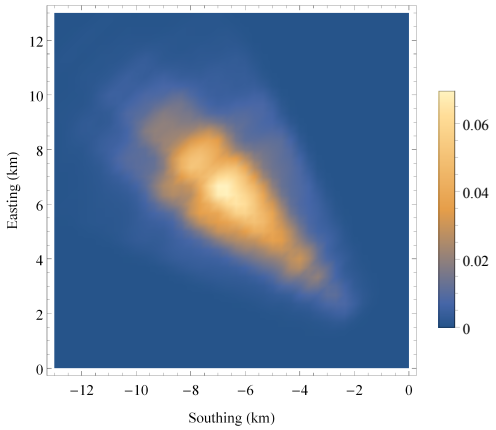

Figure 12: Probability density function of the landing coordinates resulting from the Monte Carlo simulation.

of the landing sites is represented. Furthermore, this figure enables us to distinguish better the most probable landing area since Fig.(11) gets saturated in this region due to the great amount of trajectories simulated.

The confidence ellipses in Fig.(11) are rather eccentric. Their major axes (aligned northeastward) measure 10.4 km, for a confidence of 95%, and 9.1 km, for 90% of confidence. As the furthest landing site, collinear with the major axes, is 14.6 km away from the launch location, the major axis from the lowest confidence level represents almost two thirds of the furthest distance. Thus, we conclude the measured wind speed, allied with the surface roughness length range, brings a strong uncertainty to the landing site estimation under the specified conditions. Regarding the minor axes compared to their distances from the launch site, we see that the wind direction also induces a considerable uncertainty.

5.2. Rocket design optimization

Taking the previous simulation from a different approach, we get another tool that allows us to perform optimization. Thus, after defining an optimization criteria (maximization or minimization of an output) given an universe of input variables, we can deduce the best alternative that matches our goal.

Changing the rocket parameters in each Monte Carlo iteration (opposing to the previous simulation, where the rocket properties are kept constant), we can optimize the rocket characteristics. For example, we are aiming to determine the best body tube's length and diameter combination so that the rocket reaches the highest apogee keeping constant the other properties. To this example a windless atmosphere is defined and three options for each tube's dimension, which are selected randomly from an uniform distribution. The minimum and maximum length limits (constraints) are 1 m and 2.5 m, respectively, and for the diameter are 7.5 cm and 13 cm, respectively.

In Fig.(13) the altitude over time is depicted (until the highest apogee's instant) of these nine configurations. . As shown, the configuration with the

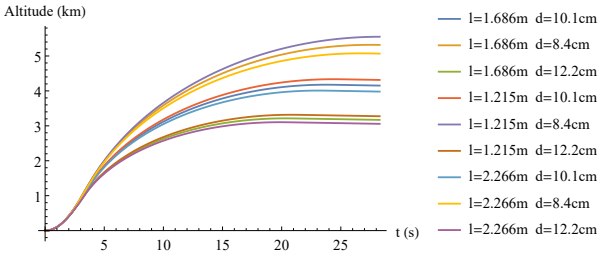

Figure 13: Altitude over time from nine launches with different rocket's length and diameter configurations.

smaller dimensions (1.215 m and 8.4 cm) reaches the highest apogee, as opposed to the rocket with the largest dimensions that reach the lowest apogee. These facts are expected due to the major influence of the rocket's dimensions on the drag coefficient and the reference area. The longer and larger the rocket is, the greater is the drag that decreases the velocity and forces the rocket to reach sooner a lower apogee. From this result, we may say this method works properly but a more extensive optimization should be performed in the future since the geometric parameters of the rocket also influence the mass of the components.

Even though this is a simple and expected example, it gives a glimpse of the many possibilities at our disposal after developing a Monte Carlo simulation to our tool. From this starting point, and having enough computational resources, more complex

optimizations may be processed. Besides, other efficient optimization methods (not considered in this work) may be developed and applied to the presented tool so that the expected result can be fast and directly found, saving resources finding the best alternative from the outputs.

6. Conclusions

The present work focused on the development of a trajectory simulator tool for fin-stabilized model and sounding rockets addressing the effects of an ABL profile. This tool was developed under *Mathematica*® and supports from model to sounding rockets with any number of stages. This work presented the tool's flexibility to customize the default models and to compute the outcome from the inputs' uncertainties (or perform an optimization) from a Monte Carlo simulation.

The developed structure to describe the rocket was presented and is adaptable to any type of common rockets. The developed atmospheric model takes into account the local conditions at the launch site which tend to the CIRA-86 profile at a specified rate. Likewise, above the ABL, the wind model approximates the values given in the CIRA-86 tables. Within the ABL, as the wind plays an important role in the model rockets trajectory, three profiles were implemented considering the atmospheric stability, which can be deduced from the Obukhov length. As this parameter is hard to determine with low errors using common measuring instruments, a qualitative alternative was presented to figure out the atmospheric stability from the weather conditions. Besides the local atmospheric data, the ABL profiles also take into account the type of the surface. In order to improve the simulations considering the rocket's attitude, as our tool possesses three degrees of freedom, we developed a model to compute the angle of attack over time that can be influenced by wind gusts appearing along the wind direction. A drag coefficient model was also implemented depending on the Mach, the Reynolds and the configuration of the rocket.

A simulation from a model rocket launch was performed in order to present examples from the tool's outputs. The results revealed a large impact of the wind in the trajectories (due to the weathercock effect), which leads us to reassure the importance to forecast the atmospheric stability and to model a suitable wind profile. Exploring the potentialities from the tool, from a Monte Carlo simulation, we also conclude that the wind profiles must always concern the local conditions at the launch since, for the defined uncertainties, they impose a strong influence in estimating the landing site. Using the same simulation process, we also presented a method to optimize the rocket characteristics which showed expected results.

References

[1] Degeratu, M., Georgescu, A. M., Bandoc, G., Alboiu, N. I., Cosoiu, C. I., and Golumbeanu, M. Atmospheric Boundary Layer Modelling as Mean Velocity Profile Used for Wind Tunnel Tests on Contaminant Dispersion in the Atmosphere. *Journal of Environmental Protection and Ecology*, 14(1):22–28, 2013.

[2] Thuillier, R. H. and Lappe, U. Wind and Temperature Profile Characteristics from Observations on a 1400 ft Tower. *Journal of Applied Meteorology*, 3:299–306, June 1964.

[3] Seibert, G. *The History of Sounding Rockets and Their Contribution to European Space Research.* ESA Publications Division, November 2006.

[4] Wolfram Research, Inc., Mathematica, Version 10.2, Champaign, IL (2015).

[5] Barrowman, J. Stability of a Model Rocket in Flight. Technical Information Report 30, Centuri Engineering Company, 1970.

[6] Stull, R. *An Introduction to Boundary Layer Meteorology.* Kluwer Academic Publishers, 1988.

[7] Tennekes, H. The Logarithmic Wind Profile. *Journal of the Atmospheric Sciences*, 30(2):234–238, March 1973.

[8] Arya, S. P. *Introduction to Micrometeorology.* Academic Press, Inc., 1988.

[9] Gryning, S. E., Batchvarova, E., Brümmer, B., Jørgensen, H., and Larsen, S. On the extension of the wind profile over homogeneous terrain beyond the surface boundary layer. *Boundary-Layer Meteorology*, 124(2):251–268, August 2007.

[10] Tewari, A. *Atmospheric and Space Flight Dynamics.* Birkhauser, 2007.

[11] Feodosiev, V. I. and Siniarev, G. B. *Introduction to Rocket Technology.* Academic Press Inc., 1959.

[12] Milligan, T. Basics of Dynamic Flight Analysis (Part 3) - The Damping Moment Coefficient. *Peak of Flight Newsletter*, (195), October 2007.

[13] Curtis, H. *Orbital Mechanics for Engineering Students.* Elsevier, 2nd edition, 2010.

[14] Raychaudhuri, S. Introduction to Monte Carlo simulation. In *Proceedings of the 2008 Winter Simulation Conference*, pages 91–100, 2008.